ANALIZA DEFORMACIJE JEZU Z ROBUSTNIMI UTEŽNIMI FUNKCIJAMI

ANALYSIS OF DAM DEFORMATION WITH ROBUST WEIGHT FUNCTIONS

Berkant Konakoğlu

UDK: 528.48:627.82(560Deriner):
Klasifikacija prispevka po COBISS.SI: 1.01
Prispelo: 24. 4. 2020
Sprejeto: 12. 6. 2020

DOI: 10.15292/geodetski-vestnik.2020.02.198-213
SCIENTIFIC ARTICLE
Received: 24. 4. 2020
Accepted: 12. 6. 2020

IZVLEČEK

Gradbeni objekti, kot so mostovi in jezovi, so izpostavljeni različnim deformacijam, ki jih moramo stalno spremljati. V preteklosti so bili razviti različni pristopi za preučevanje obnašanja grajenega ali naravnega objekta. Najpomembnejša naloga pri deformacijski analizi je določiti, ali so točke stabilne ali nestabilne. V raziskavi so bile uporabljene različne robustne utežne funkcije za določitev stabilnosti oziroma nestabilnosti točk na primeru jezu Deriner, pri čemer smo uporabili podatke opazovanj GNSS (angl. Global Navigation Satellite System*) iz štirih terminskih izmer. Pri tem smo uporabili Andrewsovo, Beaton-Tukeyjevo, Cauchyjevo, dansko, Fairovo, German-McClurejevo, Hampelovo, Huberjevo, L1 in L1–L2 robustno funkcijo. Na podlagi rezultatov izračunov smo ocenili lastnosti uporabljenih metod deformacijske analize. Ne glede na metodo, ki je bila uporabljena, se je izkazalo, da so skoraj vse opazovane točke na jezu Deriner v obravnavanem 1,5-letnem obdobju nestabilne. Položaji točk so bili nedvoumno pod vplivom vodne obremenitve. Izkazalo se je tudi, da so horizontalni premiki opazovanih točk, ki so bili določeni na podlagi opazovanj GNSS in robustnih utežnih funkcij, podobni za vse uporabljene metode – izjema so rezultati izračuna po metodi L1–L2. Vsi ti rezultati so bili primerjani še z izračuni po metodi θ^2. Glede na izračune, pridobljene po tej metodi, lahko ugotovimo, da so rezultati primerljivi, čeprav je bila v preteklosti metoda θ^2 obravnavana kot primernejša.*

KLJUČNE BESEDE

deformacijska analiza, GNSS, stabilnost točke, robustna utežna funkcija, jez Deriner

ABSTRACT

Civil engineering structures (e.g., bridges, dams) are exposed to deformation under the influence of various factors such as water level changes, landslides, tectonic phenomena, etc. These deformations must be periodically monitored. Various deformation analysis approaches have been developed to describe the behaviour of a structure or natural process. The most significant task in deformation analysis is to correctly classify whether the points are stable or unstable. In this study, various robust weight functions for determination of stable/unstable points were applied to the Deriner Dam using GNSS (Global Navigation Satellite System) data measured over four different periods. The robust weight functions examined included the Andrews, Beaton–Tukey, Cauchy, Danish, Fair, German–McClure, Hampel, Huber, L1, and L1–L2. Test results were evaluated, and the performances of the different deformation analysis methods were determined. It was concluded that the horizontal deformations based on GNSS data determined by these robust weight functions were in good agreement with each other, except for the L1–L2. The results of all approaches were also compared with the results of the θ^2–Criteria method. According to the results obtained, although the θ^2–Criteria and the robust methods yielded nearly similar results, the results of the θ^2–Criteria method were thought to be more reliable.

KEY WORDS

Deformation analysis, GNSS, Point stability, Robust weight functions, Deriner Dam

1 INTRODUCTION

In Turkey, dams established with very substantial financial resources are the most important facilities for the management of our water. Dams are the structures that provide society with many different benefits such as energy, irrigation water, flood control, and recreational facilities. However, to ensure the sustainability of these benefits and to prevent future disasters, the existing dams must be safely operated and managed. Dam safety plays an important role in increasing the efficiency of these facilities. Geodetic and geotechnical/structural methods are used to carry out investigations into possible deformation (Setan and Sing, 2001; Setan et al., 2003; Erol et al., 2004). The non–geodetic (geotechnical) methods use instruments such as accelerometers, extensometers, inclinometers, magnetic columns, piezometers, tiltmeters, pendulums, vibration meters, and strainmeters (Amiri-Simkooei et al., 2017). The geodetic method is based on geodetic networks that are established and periodically measured using different methods (i.e., total station measurements, levelling, GNSS) (Scaioni et al., 2018). The object or area under investigation is represented by several points consisting of stable landmarks or marked locations. The points are then measured at least twice more at different times, and the results analysed. Statistically significant displacements are evaluated using deformation analysis methods found in the literature, including those based on the congruency test (Niemeier, 1981; Pelzer, 1971, 1974) and methods based on robust estimation, specifically on the robust M–estimation (Nowel, 2015a, 2015b; Nowel and Kamiński, 2014), the M–split estimation (Duchnowski and Wiśniewski, 2012; Wiśniewski, 2009, 2010) and the R–estimation (Duchnowski, 2013; Duchnowski and Wiśniewski, 2017).

A wealth of studies can be found in the literature covering geodetic deformation monitoring for stability and safety in various types of dams (Acosta et al., 2018; Alcay et al., 2018; Barzaghi et al., 2018; Bayrak, 2008; Gikas and Sakellariou, 2008; Guler et al., 2006; Kalkan, 2014; Manake and Kulkarni, 2002; Saidi et al., 2017; Taşçi, 2008; Xiao et al., 2019). Bayrak (2007) evaluated the vertical displacements of the Yamula Dam based on terrestrial geodetic measurement operations during the first filling of the reservoir. Six reference and nine object points were utilised to detect the vertical movements. A total station (Sokkia 530R) was used to collect the height data. Measurements were carried out over four periods (December 2003, March 2004, November 2004 and April 2005). The free network adjustment technique was applied to adjust each measurement period. Geodetic measurements were then analysed using models based on the static global congruency test, the kinematic Kalman–Filter, and the dynamic Kalman–Filter. Each model yielded consistent results. The results indicated that reservoir water level changes were a significant triggering factor for Yamula Dam deformation. Besides, compared to other deformation models, the developed dynamic model presented the relationship between the vertical movements and the reservoir level changes. Taşçi (2010) evaluated the horizontal displacements of the Altinkaya Dam by means of the GPS (Global Positioning System) measurement technique. To monitor the displacements, six reference and ten object points were installed at the dam crest and around it. The first measurement operation was performed on 21 September 2000. Three more measurement assessments were then carried out (5 May 2001, 20 September 2001, and 27 May 2002). The iterative weighted similarity transformation, least absolute sum, congruency test, and Fredericton approach were utilised to determine the stable/unstable points. The points with a horizontal displacement greater than or equal to 4 mm were considered as unstable. The results also showed that horizontal displacements could occur in the middle part of the dam caused by the reservoir water level. Yigit et al. (2016) established a geodetic network of ten reference

and nineteen object points to investigate the horizontal deformations at the crest of the Ermenek Dam. In their study, a conventional measurement method (a total station with a prism) and a conventional deformation analysis technique were used and Pope's test was adopted to detect outlying observation(s). The results indicated that there was a correlation between relative movements and reservoir water load. Furthermore, it was concluded that a 58–m increase in water level caused a movement of about 1 cm on the dam crest. Yavaşoğlu et al. (2018) investigated the long-term (over ten years) behaviour of the Atatürk Dam on the Euphrates River in Turkey. Conventional and GNSS (Global Navigation Satellite System) data were used to monitor measured deformations. Furthermore, conventional deformation and strain analysis were also applied. It was concluded that the strain and deformation analysis results were compatible with each other. The results also demonstrated that the dam body had become more stable, and the displacement rate of the dam had decreased significantly despite the increase in the water load. Using GNSS, Konakoglu et al. (2020) evaluated the horizontal and vertical movements of Deriner Dam analysed using the θ^2–Criteria (classical deformation) method to determine the statistically displaced points in a geodetic deformation network. They found significant horizontal and vertical movements on the dam crest. However, the vertical movements were deemed erroneous because they were higher than expected. Only the θ^2–Criteria method was used to detect stable/unstable points in the Deriner Dam.

The aim of this present study was to evaluate the horizontal displacements of the Deriner Dam using ten different robust weight functions. In view of the above, the Andrews, Beaton–Tukey, Cauchy, Danish, Fair, German–McClure, Hampel, Huber, L1, and L1–L2 robust weight functions were applied. The performances of these functions were investigated to evaluate their behaviours and similarities in the detection of existing deformations. Afterwards, the results were compared with those of the θ^2–Criteria method.

This paper is organised as follows. The introduction section provides a brief review of the ten weight functions used for detecting stable/unstable points in a geodetic deformation network: the Andrews, Beaton–Tukey, Cauchy, Danish, Fair, German–McClure, Hampel, Huber, L1, and L1–L2. The following section introduces the study area, the geodetic deformation network used, and the GNSS measurements. The subsequent section presents the results based on the deformation analyses, and the findings are discussed by comparing them with the results of the θ^2–Criteria method. Finally, some conclusions are given in the last section.

2 ROBUST METHODS

Robust methods have been applied in scientific fields more frequently after the publication of Huber's article (Huber, 1964). These methods are used to predict the tendency of point displacing and have a wide range of applications for deformation detection. Robust methods are based on the S–transformation (Helmert's similarity transformation), as expressed in Eq. (1).

$$\left.\begin{aligned} \hat{\boldsymbol{d}}^{(k)} &= \boldsymbol{S}^{(k)}\boldsymbol{d} \\ \boldsymbol{Q}_{\hat{\boldsymbol{d}}}^{(k)} &= \boldsymbol{S}^{(k)}\boldsymbol{Q}_{\boldsymbol{d}}\left(\boldsymbol{S}^{(k)}\right)^{\boldsymbol{T}} \\ \boldsymbol{W}^{(k+1)} &= diag(\ldots, w_i^{(k+1)}, \ldots) \end{aligned}\right\}_{k=1,2,\ldots} \tag{1}$$

where $\boldsymbol{d}$ = the displacement vector; $\boldsymbol{Q}_{\boldsymbol{d}}$ = its cofactor matrix; $\boldsymbol{S}^{(k)} = \boldsymbol{I} - \boldsymbol{Q}(\boldsymbol{H}^T\boldsymbol{W}^{(k)}\boldsymbol{H})^{-1}\boldsymbol{H}^T\boldsymbol{W}^{(k)}$; $\boldsymbol{I}$ = the identity matrix; and $\boldsymbol{H}$ = the inner constraints datum matrix, which spans the null space of the design matrix. In the first iteration ($\boldsymbol{k} = 1$), the weight matrix is accepted as $\boldsymbol{W}^{(k)} = \boldsymbol{I}$ (Setan and Singh, 2001).

Several robust weight functions have been proposed and commonly used to solve geodetic problems. For example, if the Huber weight function is adopted for the displacement problem, in the subsequent iterations, the weights of the points will be determined as shown in Eq. (2) (Chen, 1983; Chen et al., 1990).

$$w_i = \begin{cases} 1 & \left|\hat{d}_i\right| \le q_i \\ \dfrac{q_i}{\left|\hat{d}_i\right|} & \left|\hat{d}_i\right| > q_i \end{cases} \tag{2}$$

where $\hat{d}_i =$ the given component of vector $\boldsymbol{d}$ for point $i\left(\hat{d}_{x_i}\text{ or }\hat{d}_{y_i}\right)$; $q_i = c\hat{\sigma}_{\hat{d}_i}$ is the tuning constant; c = a suitable factor (e.g., = 1.5); and $\hat{\sigma}_{\hat{d}_i}$ = the standard deviation estimate for the corresponding component of the displacement vector $\hat{d}_i\left(\hat{\sigma}_{\hat{d}_{x_i}}\text{ or }\hat{\sigma}_{\hat{d}_{y_i}}\right)$.

The displacement vector components depend on the orientation of the reference system of the network, which is determined by approximate coordinates. Caspary and Borutta (1987), Caspary et al. (1990), and Caspary (2000) proposed that the best solution may be for the weight function variables to be the lengths of the displacement vectors. For example, if the Huber weight function is the weight function and the variables are in the form of the lengths of the displacement vectors, then the weight function will take this form, as in Eq. (3).

$$w_i = \begin{cases} 1 & \left|\hat{s}_i\right| \le q_i \\ \dfrac{q_i}{\left|s_i\right|} & \left|\hat{s}_i\right| > q_i \end{cases} \tag{3}$$

where $\hat{s}_i = \sqrt{\hat{d}_{x_i}^2 + \hat{d}_{y_i}^2}$; $q_i = c\sigma_{\hat{s}_i}$; and $\hat{\sigma}_{\hat{s}_i}^2 = \left(\dfrac{\hat{d}_{x_i}}{\hat{s}_i}\right)^2 \hat{\sigma}_{\hat{d}_{x_i}}^2 + 2\dfrac{\hat{d}_{x_i}}{\hat{s}_i}\dfrac{\hat{d}_{y_i}}{\hat{s}_i}\hat{\sigma}_{\hat{d}_{x_i}\hat{d}_{y_i}}^2 + \left(\dfrac{\hat{d}_{y_i}}{\hat{s}_i}\right)^2 \hat{\sigma}_{\hat{d}_{y_i}}^2$ (e.g. Savšek-Safić et al., 2006).

The iterative procedure given in Eq. (1) continues until the differences between the displacements of all common points $\left|\boldsymbol{d}^{(k+1)} - \boldsymbol{d}^{(k)}\right|$ are less than the tolerance value ε (i.e., 0.0001 m.).

2.1 Other weight functions of robust methods used in this study

– Andrews weight function (Andrews, 1974)
  The Andrews weight function assumes the form of Eq. (4).

$$w_i = \begin{cases} \left(\sin\dfrac{\hat{s}_i}{q_i}\left(\dfrac{\hat{s}_i}{q_i}\right)^{-1}\right. & \left|\hat{s}_i\right| \le q_i\pi \\ 0 & \left|\hat{s}_i\right| > q_i\pi \end{cases} \tag{4}$$

  where $q_i = c\hat{\sigma}_{\hat{s}_i}$; c = 1.5.

– Beaton–Tukey weight function (Beaton and Tukey, 1974)
  The Beaton–Tukey weight function assumes the form of Eq. (5).

$$w_i = \begin{cases} \left[1 - \left(\frac{\hat{s}_i}{q_i}\right)^2\right]^2 & |\hat{s}_i| \le q_i \\ 0 & |\hat{s}_i| > q_i \end{cases} \tag{5}$$

where $q_i = c\hat{\sigma}_{\hat{s}_i}$; $c = 1.5$.

– Cauchy weight function (Pennacchi, 2008)
The Cauchy weight function assumes the form of Eq. (6).

$$w_i = \frac{1}{1 + \left(\frac{|\hat{s}_i|}{q_i}\right)^2} \tag{6}$$

where $q_i = c\hat{\sigma}_{\hat{s}_i}$; $c = 2.3849$.

– Danish weight function (Berberan, 1992)
The Danish weight function assumes the form of Eq. (7).

$$w_i = \begin{cases} 1 & |\hat{s}_i| \le q_i \\ exp\left(-\frac{\hat{s}_i^2}{q_i^2}\right) & |\hat{s}_i| > q_i \end{cases} \tag{7}$$

where $q_i = c\hat{\sigma}_{\hat{s}_i}$; $c = 3$.

– Fair weight function (Pennacchi, 2008)
The fair weight function assumes the form of Eq. (8).

$$w_i = \frac{1}{1 + \frac{|\hat{s}_i|}{q_i}} \tag{8}$$

where $q_i = c\hat{\sigma}_{\hat{s}_i}$; $c = 1.3998$.

– German–McClure weight function (Pennacchi, 2008)
The German–McClure weight function assumes the form of Eq. (9).

$$w_i = \frac{1}{\left(1 + (\hat{s}_i)^2\right)^2} \tag{9}$$

– Hampel weight function (Hampel et al., 1986)
The Hampel weight function assumes the form of Eq. (10).

$$w_i = \begin{cases} 1 & 0 < |\hat{s}_i| \le q_i \\ \frac{q_i}{|\hat{s}_i|} & q_i < |\hat{s}_i| \le u_i \\ \frac{q_i\left(v_i - |\hat{s}_i|\right)}{|\hat{s}_i|\left(v_i - u_i\right)} & u_i < |\hat{s}_i| \le v_i \\ 0 & |\hat{s}_i| > v_i \end{cases} \tag{10}$$

where $q_i = a\hat{\sigma}_{\hat{s}_i}$; $u_i = b\hat{\sigma}_{\hat{s}_i}$; $v_i = c\hat{\sigma}_{\hat{s}_i}$; a = 1.5; b = 3; and c = 6(Erenoglu and Hekimoglu 2007).

– L1 weight function (Pennacchi, 2008)
The L1 weight function assumes the form of Eq. (11).

$$w_i = \frac{1}{\left|\hat{s}_i\right|} \tag{11}$$

– L1–L2 weight function (Pennacchi, 2008)
The L1–L2 weight function assumes the form of Eq. (12).

$$w_i = \frac{1}{\sqrt{1+\frac{\left(\hat{s}_i\right)^2}{2}}} \tag{12}$$

Two hypotheses were proposed to investigate whether there were any statistically significant movements during the time span between two periods: the null hypothesis ($\boldsymbol{H_0}$) and the alternative hypothesis ($\boldsymbol{H_A}$), expressed as Eqs. (13) and (14), respectively.

$$\boldsymbol{H_0 : E(\hat{d}) = E(\hat{x}_2) - E(\hat{x}_1) = 0} \tag{13}$$

and

$$\boldsymbol{H_A : E(\hat{d}) = E(\hat{x}_2) - E(\hat{x}_1) \neq 0} \tag{14}$$

where $\boldsymbol{E}$ = the expectation operator. If $\boldsymbol{H_0}$ is true, it means that there was no significant deformation for any of the geodetic network points. In the opposite case, a group of geodetic network points did not remain stable during the time span between the two periods and the final displacement vector $\boldsymbol{d}$ and its final cofactor matrix $\boldsymbol{Q_d}$ are obtained from the final iteration.

In order to decide whether or not $\hat{d}_i$ might be interpreted as displacement, the test formula was set as in Eq. (15).

$$T_i = \frac{\left(\hat{d}_i^{(k+1)}\right)^T \left(Q_{\hat{d}_i}^{(k+1)}\right)^{-1} \hat{d}_i^{(k+1)}}{\hat{\sigma}_0^2 h_i} \sim F\left(1-a, h_i, f\right) \tag{15}$$

where $\hat{\boldsymbol{\sigma}}_{\boldsymbol{0}}^{\boldsymbol{2}}$ = the pooled variance factor estimator for the two measurement periods; F = Fisher's distribution; a = the significance level (generally a = 0.05); $h_i = rank\left(Q_{\hat{d}_i}^{-1}\right)$; and f = the number degrees of freedom for all measurement periods. If the aforementioned test is failed (i.e., $T_i > F(1 - a, h_i, f)$, this means that point i can be regarded as unstable; otherwise, it can be stated that this point was not significantly displaced.

3 STUDY AREA, GEODETIC DEFORMATION NETWORK USED AND GNSS MEASUREMENTS

The Deriner Dam, which is a double–curvature concrete dam, was constructed in the north-eastern Black Sea Region of Turkey (Fig. 1). This structure is one of the highest arc dams in the world. It was built under the Coruh River Basin master plan. This plan includes 30 dams. The Deriner project was begun in 1998 and completed in 2013 and has a designed maximum storage capacity of 1.970 million m^3. The height of the Deriner Dam is 249 m and its crest length is 720 m, with the crest width of the crown

cantilever measuring 12 m. The dam provides a significant amount of energy to Turkey. With its four vertical energy generation units, the dam is estimated to produce 2,300 GWh of electrical energy annually.

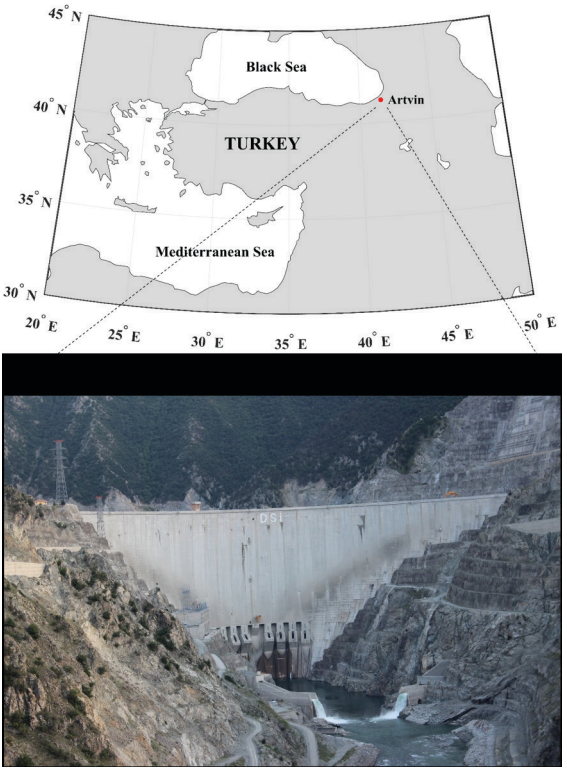

Figure 1: Location of Artvin and the Deriner Dam.

The geodetic deformation network consists of twelve reference and seven object points used to monitor the displacements via GNSS. Figure 2 presents the location of the reference and object points in the study area.

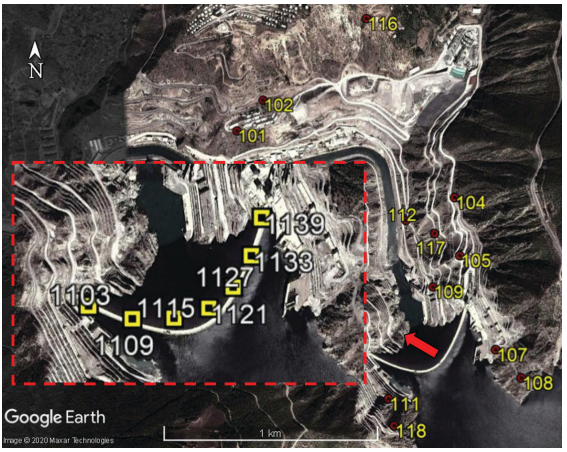

Figure 2: Reference and object points shown in Google Earth (Image ©2020 Maxar Technologies).

Four measurement operations were performed on the geodetic deformation network (May 2016, November 2016, May 2017, and August 2017). Each measurement operation was carried out on 2 consecutive days. Static GNSS observations were conducted in the points of this geodetic deformation network. The observation duration was set for at least two hours and one hour for the reference and object points. The elevation cut−off angle and the data-sampling rate was set to 15° and 10 sec, respectively. Four HiPer Pro and four GR5 receivers were used for all periods. Attention was paid to use GNSS receivers at the same points in all measurement periods. The GNSS receivers installed on a concrete pillar can be seen in Figure 3.

Figure 3: GNSS receivers on reference points 117 (left) and 104 (right).

The GNSS measurements were post-processed via the Magnet Tools 5.1 software. The Cartesian coordinate differences and cofactor matrices of these differences were then obtained. This software can give geocentric Cartesian coordinates in the World Geodetic System 1984 (WGS84) datum. In order to see the real direction of the displacement, all WGS84 geocentric Cartesian coordinates had to be transformed into the local topocentric coordinate system. The point 1139 was chosen as the origin of the topocentric coordinate system. For more information about the transformation procedure, one may refer to Yigit (2016). Each period was adjusted separately using the free network adjustment technique. The Huber M-estimation method was used to determine the outlying observation(s) (Huber, 1981). Since the vertical displacements in Konakoglu et al. (2020) were found to be erroneous, the vertical displacements were not analysed in this study. Water levels were about 389 m in May 2016, 377 m in November 2016, 364 m in May 2017, and 374 m in August 2017.

4 RESULTS AND DISCUSSION

To determine the displaced points in the Deriner Dam geodetic deformation network, a comparative analysis was carried out using ten different robust weight functions. The May 2016 period was taken as the reference period. First, the horizontal displacements (***d***) and test values (***T***) were calculated. Subsequently, the test values were compared with the F–distribution table to determine whether or not the displacements of the points were significant. The results of the reference and object points for the periods May–November 2016, May 2016–May 2017, and May 2016–August 2017 are given in Tables 1, 2, and 3, respectively. The stable or unstable expression of a point is shown in the decision column in the tables. If the point had significantly changed, the (✓) sign denotes "unstable"; otherwise, the (×) sign indicates "stable". Test values (***T***) are also given in Figures 4, 5, and 6 for the periods May–November 2016, May 2016–May 2017, and May 2016–August 2017, respectively.

According to the results of the deformation analyses performed with different robust weight functions during the period between May and November 2016 (Table 1), the number of points determined as unstable included: 9 points with the Andrews, Beaton–Tukey, Cauchy, and Danish methods, 10 points with the Huber method, 14 points with the L1 method, 15 points with the German–McClure and Hampel methods, and 16 points with the Fair and L1–L2 methods. The Fair, German–McClure, Hampel, L1, and L1–L2 methods found almost the same number of points to be unstable during this period.

According to the results of the deformation analyses performed with different robust weight functions during the period between May 2016 and May 2017 (Table 2), the number of points determined as unstable included: 10 points with the Andrews, Beaton–Tukey, Cauchy, Danish, German–McClure, Hampel and L1 methods, 11 points with the Huber method, and 12 points with the Fair and L1–L2 methods. All robust methods determined the number of unstable points to be between 10 and 12 during this period.

According to the results of the deformation analyses performed with different robust weight functions during the period between May 2016 and August 2017 (Table 3), the number of points determined as unstable included: 7 points with the Cauchy, Danish, Hampel, and Huber methods, 9 points with the Fair method, German–McClure, and L1 methods, 10 points with the Andrews method, 12 points with the Beaton–Tukey method, and 15 points with the L1–L2 method. The Andrews, Beaton–Tukey, Cauchy, and Danish robust methods detected nearly the same number of unstable points, except for the period between May 2016 and August 2017. The reason for this difference may be that the test values of the unstable points in the period between May 2016 and August 2017 were very close to each other, but below the tolerance value.

By comparing the results of all the robust weight functions, the values of the displacement magnitudes calculated with the L1–L2 method were generally found to be higher than those of the other methods. Thus, this method detected many more unstable points compared with the other methods. This can be clearly seen from the calculated test values shown in Tables 1, 2, and 3.

Significant displacements were seen at object points 1115, 1121, and 1127, which are in the middle of the dam crest. Considering all the GNSS measurements performed in all periods, the largest horizontal

displacement (i.e., 2.60 cm) was experienced at object point 1121 at the middle of the dam crest. It was also seen that the horizontal displacements gradually decreased towards the right and left abutments. Despite this decrease, the horizontal displacements for object points 1103 and 1139 reached an average of 6–7 mm between the periods of May 2016 and May 2017. This may demonstrate that the left and right abutment sections of the dam were not rigid between these periods. Starting from May 2016 up to May 2017, the reservoir water level had dropped about 25 m. That was the reason for the excessive displacement on the left and right abutments. Although there was an increased difference in the reservoir water level from May 2016 to May 2017, a slowdown was observed in the displacements of the object points at the middle part of the dam.

Between the periods of May 2016 and November 2016, the horizontal displacements for object points 1103 and 1139 did not exceed about 3–4 mm in any of the models except L1 and L1–L2.

According to the results of the deformation analyses performed with different robust weight functions, the reference point 102 was determined as unstable in all period comparisons. Moreover, for the period between May 2016 and May 2017 reference point, 112 was detected to be unstable based on the results of all methods. The reference points are thought to act for another reason, considering that they are not affected by the water load.

The amounts of horizontal displacement for the periods May 2016–November 2016 and May 2016–August 2017 are very similar. The reason for this situation may be that the November 2016 and August 2017 periods had almost the same water levels.

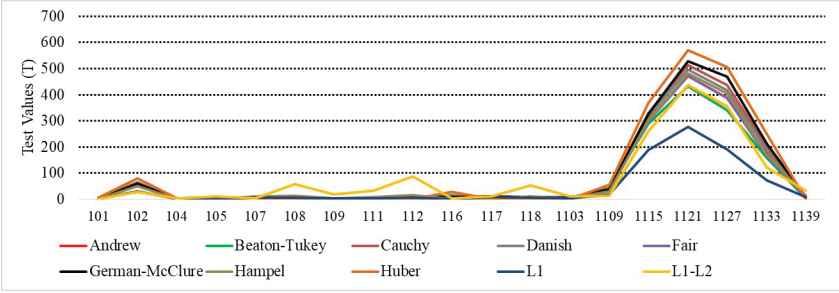

Figure 4: Calculated test values May 2016–November 2016.

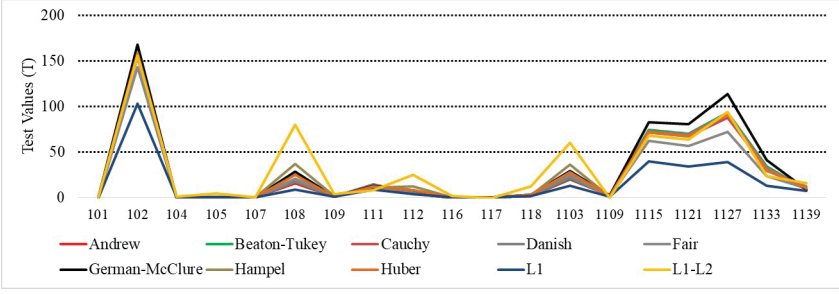

Figure 5: Calculated test values May 2016–May 2017.

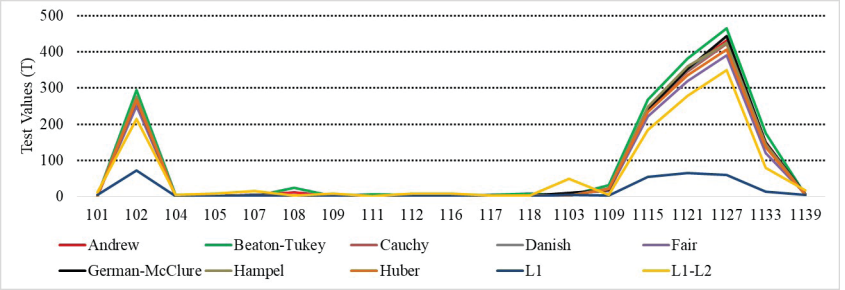

Figure 6: Calculated test values May 2016–August 2017.

Table 1: Deformation analysis with the ten robust weight functions for May 2016 – November 2016.

		Andrews		Beaton-Tukey		Cauchy		Danish		Fair		German-McClure		Hampel		Huber		L1		L1–L2	
	PN	***d***	Dec.	***d***	Dec.	***d***	Dec.	***d***	Dec.	***d***	Dec.	***d***	Dec.	***d***	Dec.	***d***	Dec.	***d***	Dec.	***d***	Dec.
Reference Points	101	0.26	✓	0.33	✓	0.25	✓	0.25	✓	0.14	×	0.16	×	0.10	×	0.35	✓	0.09	×	–0.12	×
	102	0.93	✓	0.99	✓	0.92	✓	0.91	✓	0.80	✓	0.82	✓	0.77	✓	1.02	✓	0.75	✓	0.54	✓
	104	0.18	×	0.25	×	0.17	×	0.17	×	0.06	×	0.08	×	0.03	×	0.27	✓	0.01	×	–0.20	×
	105	0.11	×	0.18	×	0.10	×	0.09	×	–0.01	×	0.01	×	–0.05	×	0.20	✓	–0.06	×	–0.27	✓
	107	–0.09	×	–0.02	×	–0.10	×	–0.10	×	–0.21	✓	–0.19	✓	–0.25	×	0.00	×	–0.26	✓	–0.47	✓
	108	–0.09	×	–0.02	×	–0.10	×	–0.10	×	–0.21	✓	–0.19	✓	–0.25	✓	0.00	×	–0.26	✓	–0.47	✓
	109	–0.05	×	0.02	×	–0.06	×	–0.06	×	–0.17	✓	–0.15	×	–0.20	✓	0.04	×	–0.22	×	–0.43	✓
	111	–0.06	×	0.01	×	–0.07	×	–0.07	×	–0.18	✓	–0.16	✓	–0.21	✓	0.03	×	–0.23	✓	–0.44	✓
	112	–0.07	×	0.00	×	–0.08	×	–0.09	×	–0.19	✓	–0.17	✓	–0.23	✓	0.02	×	–0.24	✓	–0.45	✓
	116	0.29	✓	0.35	✓	0.28	✓	0.27	✓	0.16	✓	0.18	✓	0.13	×	0.38	✓	0.11	×	–0.10	×
	117	–0.10	×	–0.03	×	–0.11	×	–0.12	×	–0.22	✓	–0.20	✓	–0.26	✓	–0.01	×	–0.27	✓	–0.48	✓
	118	–0.08	×	–0.01	×	–0.08	×	–0.09	×	–0.20	✓	–0.18	✓	–0.23	✓	0.01	×	–0.25	✓	–0.46	✓
Object Points	1103	–0.06	×	0.01	×	–0.07	×	–0.08	×	–0.18	✓	–0.16	✓	–0.22	✓	0.03	×	–0.23	✓	–0.44	✓
	1109	0.79	✓	0.85	✓	0.78	✓	0.77	✓	0.66	✓	0.68	✓	0.63	✓	0.88	✓	0.61	✓	0.40	✓
	1115	2.00	✓	2.07	✓	1.99	✓	1.99	✓	1.88	✓	1.90	✓	1.85	✓	2.09	✓	1.83	✓	1.62	✓
	1121	2.24	✓	2.30	✓	2.23	✓	2.22	✓	2.11	✓	2.13	✓	2.08	✓	2.33	✓	2.06	✓	1.86	✓
	1127	1.69	✓	1.76	✓	1.68	✓	1.68	✓	1.57	✓	1.59	✓	1.54	✓	1.78	✓	1.52	✓	1.31	✓
	1133	1.08	✓	1.15	✓	1.07	✓	1.07	✓	0.96	✓	0.98	✓	0.92	✓	1.17	✓	0.91	✓	0.70	✓
	1139	–0.22	×	–0.15	×	–0.22	✓	–0.23	✓	–0.34	✓	–0.32	✓	–0.37	✓	–0.13	×	–0.39	✓	–0.60	✓

PN = Point Number, ***d*** = horizontal displacements (cm), Dec. = Decision, the (✓) sign denotes "unstable", the (×) sign indicates "stable"

Table 2: Deformation analysis with the ten robust weight functions for May 2016 – May 2017.

		Andrews		Beaton–Tukey		Cauchy		Danish		Fair		German–McClure		Hampel		Huber		L1		L1–L2	
	PN	***d***	Dec.	***d***	Dec.	***d***	Dec.	***d***	Dec.	***d***	Dec.	***d***	Dec.	***d***	Dec.	***d***	Dec.	***d***	Dec.	***d***	Dec.
Reference Points	101	0.07	×	0.06	×	0.05	×	0.05	×	–0.01	×	0.04	×	–0.04	×	0.01	×	0.01	×	–0.15	×
	102	2.19	✓	2.18	✓	2.17	✓	2.17	✓	2.11	✓	2.15	✓	2.07	✓	2.13	✓	2.13	✓	1.96	✓
	104	0.02	×	0.01	×	0.00	×	0.00	×	–0.06	×	–0.02	×	–0.10	×	–0.04	×	–0.04	×	–0.21	×
	105	–0.04	×	–0.05	×	–0.06	×	–0.06	×	–0.12	×	–0.07	×	–0.15	×	–0.10	×	–0.10	×	–0.26	✓
	107	–0.09	×	–0.10	×	–0.11	×	–0.11	×	–0.17	×	–0.12	×	–0.20	×	–0.15	×	–0.15	×	–0.31	✓
	108	–0.38	✓	–0.39	×	–0.40	✓	–0.40	✓	–0.46	✓	–0.41	✓	–0.49	✓	–0.44	✓	–0.44	✓	–0.60	✓
	109	–0.17	×	–0.17	×	–0.19	×	–0.18	×	–0.25	✓	–0.20	×	–0.28	×	–0.23	×	–0.23	×	–0.39	✓
	111	0.79	✓	0.78	✓	0.77	✓	0.77	✓	0.71	✓	0.76	✓	0.68	✓	0.73	✓	0.73	✓	0.57	✓
	112	–0.27	✓	–0.27	✓	–0.28	✓	–0.28	✓	–0.34	✓	–0.30	✓	–0.38	✓	–0.33	✓	–0.33	×	–0.49	✓
	116	0.01	×	0.01	×	0.00	×	0.00	×	–0.06	×	–0.02	×	–0.10	×	–0.05	×	–0.04	×	–0.21	×
	117	0.20	×	0.20	×	0.19	×	0.19	×	0.13	×	0.17	×	0.09	×	0.15	×	0.15	×	–0.02	×
	118	–0.17	×	–0.17	×	–0.19	×	–0.18	×	–0.25	✓	–0.20	×	–0.28	×	–0.23	✓	–0.23	×	–0.39	✓
Object Points	1103	–0.55	✓	–0.56	✓	–0.57	✓	–0.57	✓	–0.63	✓	–0.58	✓	–0.66	✓	–0.61	✓	–0.61	✓	–0.77	✓
	1109	0.22	×	0.22	×	0.21	×	0.21	×	0.15	×	0.19	×	0.11	×	0.16	×	0.16	×	0.00	×
	1115	1.21	✓	1.21	✓	1.19	✓	1.20	✓	1.13	✓	1.18	✓	1.10	✓	1.15	✓	1.15	✓	0.99	✓
	1121	1.07	✓	1.06	✓	1.05	✓	1.05	✓	0.99	✓	1.04	✓	0.96	✓	1.01	✓	1.01	✓	0.85	✓
	1127	1.06	✓	1.06	✓	1.04	✓	1.05	✓	0.98	✓	1.03	✓	0.95	✓	1.00	✓	1.00	✓	0.84	✓
	1133	0.64	✓	0.63	✓	0.62	✓	0.62	✓	0.56	✓	0.61	✓	0.52	✓	0.58	✓	0.58	✓	0.41	✓
	1139	–0.67	✓	–0.67	✓	–0.68	✓	–0.68	✓	–0.74	✓	–0.70	✓	–0.78	✓	–0.73	✓	–0.73	✓	–0.89	✓

PN = Point Number, ***d*** = horizontal displacements (cm), Dec. = Decision, the (✓) sign denotes "unstable", the (×) sign indicates "stable"

Table 3: Deformation analysis with the ten robust weight functions for May 2016–August 2017.

		Andrews		Beaton–Tukey		Cauchy		Danish		Fair		German–McClure		Hampel		Huber		L1		L1–L2	
	PN	***d***	Dec.	***d***	Dec.	***d***	Dec.	***d***	Dec.	***d***	Dec.	***d***	Dec.	***d***	Dec.	***d***	Dec.	***d***	Dec.	***d***	Dec.
Reference Points	101	–0.19	×	–0.06	×	–0.23	×	–0.20	×	–0.34	×	–0.29	×	–0.24	×	–0.22	×	–0.49	✓	–0.67	✓
	102	2.75	✓	2.89	✓	2.71	✓	2.74	✓	2.60	✓	2.65	✓	2.70	✓	2.72	✓	2.45	✓	2.27	✓
	104	0.15	×	0.29	✓	0.11	×	0.14	×	0.00	×	0.05	×	0.11	×	0.12	×	–0.15	×	–0.33	✓
	105	0.02	×	0.15	×	–0.02	×	0.01	×	–0.13	×	–0.09	×	–0.03	×	–0.02	×	–0.28	×	–0.46	✓
	107	–0.25	×	–0.11	×	–0.28	×	–0.26	×	–0.39	✓	–0.35	✓	–0.29	✓	–0.28	×	–0.54	✓	–0.72	✓
	108	0.29	✓	0.43	✓	0.26	×	0.28	×	0.15	×	0.19	×	0.25	×	0.26	×	0.00	×	–0.18	×
	109	–0.01	×	0.13	×	–0.05	×	–0.02	×	–0.16	×	–0.11	×	–0.06	×	–0.04	×	–0.31	×	–0.49	✓
	111	0.31	✓	0.45	✓	0.27	×	0.30	×	0.16	×	0.21	×	0.26	×	0.28	×	0.01	×	–0.17	×
	112	0.14	×	0.28	✓	0.10	×	0.13	×	–0.01	×	0.04	×	0.10	×	0.11	×	–0.16	×	–0.34	✓
	116	–0.05	×	0.09	×	–0.08	×	–0.06	×	–0.19	×	–0.15	×	–0.09	×	–0.08	×	–0.34	×	–0.52	✓
	117	0.16	×	0.29	✓	0.12	×	0.15	×	0.01	×	0.05	×	0.11	×	0.12	×	–0.14	×	–0.32	×
	118	0.26	✓	0.40	✓	0.22	×	0.25	×	0.11	×	0.16	×	0.22	×	0.23	×	–0.04	×	–0.22	×
Object Points	1103	–0.20	×	–0.06	×	–0.23	×	–0.21	×	–0.34	✓	–0.30	✓	–0.24	×	–0.23	×	–0.49	✓	–0.67	✓
	1109	0.72	✓	0.86	✓	0.68	✓	0.71	✓	0.57	✓	0.62	✓	0.67	✓	0.69	✓	0.42	×	0.24	✓
	1115	2.34	✓	2.47	✓	2.30	✓	2.33	✓	2.19	✓	2.24	✓	2.29	✓	2.31	✓	2.04	✓	1.86	✓
	1121	2.46	✓	2.60	✓	2.42	✓	2.45	✓	2.31	✓	2.36	✓	2.42	✓	2.43	✓	2.16	✓	1.98	✓
	1127	2.30	✓	2.44	✓	2.26	✓	2.29	✓	2.15	✓	2.20	✓	2.25	✓	2.27	✓	2.00	✓	1.82	✓
	1133	1.24	✓	1.38	✓	1.21	✓	1.23	✓	1.09	✓	1.14	✓	1.20	✓	1.21	✓	0.94	✓	0.77	✓
	1139	–0.42	✓	–0.28	✓	–0.46	✓	–0.43	✓	–0.57	✓	–0.52	✓	–0.47	✓	–0.45	✓	–0.72	✓	–0.90	✓

PN = Point Number, ***d*** = horizontal displacements (cm), Dec. = Decision, the (✓) sign denotes "unstable", the (✕) sign indicates "stable"

A previous study was conducted by Konakoglu et al. (2020) using the ^{2}–Criteria method with the same GNSS data, while ten different robust weight functions were employed to detect stable/unstable points in the present study. A 3-dimensional deformation analysis was performed by Konakoglu et al. (2020). The horizontal displacement results of the ^{2}–Criteria method for the periods May 2016–November 2016, May 2016–May 2017 and May 2016–August 2017 are given in Table 4. Considering all the GNSS measurements performed in all periods, only reference point 111 was determined to be stable. Konakoglu et al. (2020) stated that the vertical displacements are larger than expected, although this is statistically significant, and this situation is unacceptable. In Table 4, the displacements indicated with an asterisk (*) are the reference and object points that are appeared to be stable in the horizontal direction (the displacement amounts are very small) even though their vertical displacements are statistically significant. Accordingly, point 112 can be considered unstable in all periods.

Table 4: Results of θ^2–Criteria method between all periods (Konakoglu et al., 2020).

	PN	May 2016–November 2016 d(cm)	May 2016–May 2017 d(cm)	May 2016–August 2017 d(cm)
Reference Points	101	0.48	0.60	0.15*
	102	1.10	2.86	3.17
	104	–	0.33	0.16*
	105	0.19*	0.68	0.15*
	107	–	0.24*	0.49
	108	0.22*	0.61	0.74
	109	0.15*	0.38	0.20
	111	–	–	–
	112	0.16*	0.15*	0.23*
	116	0.56	0.49	0.76
	117	0.02*	–	–
	118	0.04*	0.08*	0.32
Object Points	1103	–	0.63	–
	1109	0.90	1.25	1.37
	1115	2.13	1.89	2.97
	1121	2.12	1.57	2.57
	1127	1.49	1.68	2.24
	1133	1.12	1.35	1.60
	1139	0.13*	0.68	0.32

PN = Point Number

The θ^2–Criteria method and the ten different robust methods yielded consistent results in determining the horizontal displacement. According to the results of the deformation analyses performed, all methods detected displacement at reference point 102. The horizontal displacement was up to 3.17 cm with the θ^2–Criteria method, while none of the robust method findings exceeded 2.89 cm at this reference point. The results of the θ^2–Criteria differed from those of the L1–L2 method compared to other robust methods. However, some differences were also found between the θ^2–Criteria method and the ten different robust methods. For example, more points were determined to be stable in the deformation analysis made via

the robust methods compared to the θ^2–Criteria method because the vertical displacements were not examined. Points that were found to be unstable according to the θ^2–Criteria method were found to be stable via the robust methods. The displacements of reference points 105, 111, and 116 between May 2016 and May 2017 can be given as an example of this. The maximum displacement was found at object point 1115 (i.e., 2.97 cm) with the –Criteria method, whereas the largest displacement was detected at object point 1121 (i.e., 2.60 cm) by the Beaton-Tukey method. The horizontal displacements for the reference points (i.e., 107, 108, and 109) and object points (i.e., 1103 and 1139) that were detected as positive (+) according to the θ^2–Criteria method were detected as negative (–) for the same reference and object points via the robust methods.

Under normal circumstances, horizontal displacements is normally expected to be maximum in the middle of the dam crest and the displacements are expected to decrease towards the edges of the dam. The directions and amounts of the object points close to each other are expected to be the same in concrete dams. According to the direction of changes in object points 1133–1139, although the absolute displacements look the same, the directions of the points close to each other were not the same (can be seen in Table 2). In this case, it can be interpreted that the θ^2–Criteria method provided more accurate results than the robust methods. In the deformation study performed by Setan and Singh, (2001), they revealed that the classical deformation method (congruency testing) gave better results than the robust methods (least absolute sum and iterative weighted similarity transformation). This supports the above comment.

5 CONCLUSION

The main aim of this paper was to detect the stable/unstable points on the dam crest and its surrounding area by means of ten different robust weight functions. To this aim, the GNSS measurement data on the geodetic deformation network carried out for four different periods were used. The results obtained from the comparative analysis indicated that the horizontal displacements determined by these robust weight functions are in good agreement with each other, except for the L1–L2 function. This may be because the deformation was determined using the displacement vector $\hat{s}_i$ instead of the individual components $\hat{d}_{x_i}$ or $\hat{d}_{y_i}$. The four records presented for the Deriner Dam spanning a 1.5–year period showed that almost all object points were unstable. This result indicated that there was a relationship between water load and dam deformation. According to the results of the deformation analyses conducted with different robust weight functions, the maximum displacement (which reached 2.60 cm between the periods May 2016 and August 2017) was experienced at object point 1121 at the middle of the dam crest. As can be seen from the test values of the object points, their displacements were found to be higher than for the reference points, as expected. When we examined the displacement values obtained with all the weight functions, the points with a horizontal displacement greater than or equal to 2–3 mm were considered as unstable. The displacement values below these values can be accepted as measurement noise. In the current study, the results of the deformation analysis approach using the robust weight functions were for the most part compatible with the results obtained by the θ^2–Criteria method (Konakoglu et al., 2020). However, as a result of the evaluation, the θ^2–Criteria method results are thought to give more accurate results than the other (robust) methods because the θ^2–Criteria method is believed to better reflect the effect of water level change on displacement. The datum difference can be interpreted as one

of the reasons for the differences between the θ^2–Criteria method and the robust methods. Considering all period comparisons, the Beaton-Tukey model gave the closest result to the –Criteria method in terms of displacement amount. Although Caspary (2000) suggests that it might be the best solution for the lengths of displacement vectors for weight function variables, it may be better to evaluate deformation vectors separately ($\hat{d}_{x_i}$ or $\hat{d}_{y_i}$). In addition to this, deformation research can be conducted with different constant values.

Acknowledgements

The author would like to thank the Turkish General Directorate of State Hydraulic Works (DSI) and Karadeniz Technical University for providing the data used in this study.

Literature and references:

Acosta, L., de Lacy, M., Ramos, M., Cano, J., Herrera, A., Avilés, M., Gil, A. (2018). Displacements study of an earth fill dam based on high precision geodetic monitoring and numerical modeling. Sensors, 18 (5), 1369. DOI: https://doi.org/10.3390/s18051369

Alcay, S., Yigit, C. O., Inal, C., Ceylan, A. (2018). Analysis of displacement response of the Ermenek dam monitored by an integrated geodetic and pendulum system. International Journal of Civil Engineering, 16 (10), 1279–1291. DOI: https://doi.org/10.1007/s40999-017-0211-x

Amiri-Simkooei, A. R., Alaei-Tabatabaei, S. M., Zangeneh-Nejad, F., Voosoghi, B. (2017). Stability analysis of deformation-monitoring network points using simultaneous observation adjustment of two epochs. Journal of Surveying Engineering, 143 (1), 04016020. DOI: https://doi.org/10.1061/(ASCE)SU.1943-5428.0000195

Andrews, D. (1974). A Robust Method for Multiple Linear Regression. Technometrics, 16, 523–531.

Barzaghi, R., Cazzaniga, N. E., De Gaetani C. I., Pinto L., Tornatore V. (2018). Estimating and comparing dam deformation using classical and GNSS techniques. Sensors, 18 (3), 756. DOI: https://doi.org/10.3390/s18030756

Bayrak, T. (2007). Modelling the relationship between water level and vertical displacements on the Yamula Dam, Turkey. Natural Hazards and Earth System Sciences, 7 (2), 289–297. DOI: https://doi.org/10.5194/nhess-7-289-2007

Bayrak, T. (2008). Verifying pressure of water on dams, a case study. Sensors 8 (9), 5376–5385. DOI: https://doi.org/10.3390/s8095376

Beaton, A. E., Tukey J. W. (1974). The fitting of power series, meaning polynomials, illustrated on band-spectroscopic data. Technometrics 16 (2), 147–185.

Berberan, A. (1992). Outlier detection and heterogeneous observations a simulation case study. Australian Journal of Geodesy, Photogrammetry and Surveying. 56, 49–61.

Caspary, W. F., Borutta H. (1987). Robust estimation in deformation models. Survey Review, 29 (223), 29–45. DOI: https://doi.org/10.1179/sre.1987.29.223.29

Caspary, W. F., Haen, W., Borutta, H. (1990). Deformation analysis by statistical methods. Technometrics, 39 (1), 49–57.

Caspary, W. F. (2000). Concepts of network and deformation analysis, Kensington: The University of New South Wales.

Chen, Y. G., Chrzanowski, A., Secord, J. M. (1990). A strategy for the analysis of the stability of reference points in deformation surveys. CISM Journal, 44 (2),141–49. DOI: https://doi.org/10.1139/geomat-1990-0016

Chen, Y. Q. (1983). Analysis of deformation surveys – a generalised method. Fredericton: University of New Brunswick, Technical Report No. 94.

Duchnowski, R. (2013). Hodges–Lehmann estimates in deformation analyses. Journal of Geodesy, 87 (10–12), 873–884. DOI: https://doi.org/10.1007/s00190-013-0651-2

Duchnowski, R., Wiśniewski, Z. (2017). Accuracy of the Hodges–Lehmann estimates computed by applying Monte Carlo simulations. Acta Geodaetica et Geophysica, 52 (4), 511–525. DOI: https://doi.org/10.1007/s40328-016-0186-0

Duchnowski, R., Wiśniewski, Z. (2012). Estimation of the shift between parameters of functional models of geodetic observations by applying M split estimation. Journal of Surveying Engineering, 138 (1), 1–8. DOI: https://doi.org/10.1061/(ASCE)SU.1943-5428.0000062

Erenoglu, R. C., Hekimoglu, S. (2007). An investigation into robust estimation applied to correlated GPS networks. In: M.G. Sideris (Ed.) Observing our changing earth (pp. 639–644). Berlin: Springer. DOI: https://doi.org/10.1007/978-3-540-85426-5_74

Erol, S., Erol, B., Ayan, T. (2004). A general review of the deformation monitoring techniques and a case study: analysing deformations using GPS/levelling. In 20th ISPRS Congress, 12–23 July, 2004, Istanbul.

Gikas, V., Sakellariou, M. (2008). Settlement analysis of the Mornos earth dam (Greece): Evidence from numerical modeling and geodetic monitoring. Engineering Structures, 30 (11), 3074–3081. DOI: https://doi.org/10.1016/j.engstruct.2008.03.019

Guler, G., Kilic, H., Hosbas, G., Ozaydın, K. (2006). Evaluation of the movements of the dam embankments by means of geodetic and geotechnical methods. Journal of Surveying Engineering, 132 (1), 31–39. DOI: https://doi.org/10.1061/(ASCE)0733-9453(2006)132:1(31)

Hampel, F. R., Ronchetti, E. M., Rousseeuw, P. J., Stahel W.A. (1986). Robust statistics: The approach based on influence functions. New York: Wiley.

Huber, P. J. (1964). Robust estimation of a location parameter. The Annals of Mathematical Statistics, 35 (1), 73–101.

Huber, P. J. (1981). Robust statistics. New York: Wiley.

Kalkan, Y. (2014). Geodetic deformation monitoring of Ataturk Dam in Turkey. Arabian Journal of Geosciences, 7 (1), 397–405. DOI: https://doi.org/10.1007/s12517-012-0765-5

Konakoglu, B., Cakir, L., Yilmaz, V. (2020). Monitoring the deformation of a concrete dam: a case study on the Deriner Dam, Artvin, Turkey. Geomatics, Natural Hazards and Risk, 11 (1), 160–177. https://doi.org/10.1080/19475705.2020.1714755

Manake, A., Kulkarni, M. N. (2002). Study of the deformation of Koyna dam using the Global Positioning System. Survey Review, 36 (285), 497–507. DOI: https://doi.org/10.1179/sre.2002.36.285.497

Niemeier, W. (1981). Statistical tests for detecting movements in repeatedly measured geodetic networks. Developments in Geotectonics, 16, 335–351. DOI: https://doi.org/10.1016/0040-1951(81)90076-7

Nowel, K. (2015a). Investigating the efficacy of robust M estimation of deformation from observation differences. Survey Review, 48 (346), 21–30. DOI: https://doi.org/10.1080/00396265.2015.1097585

Nowel, K. (2015b). Robust M-estimation in analysis of control network deformations: Classical and new method. Journal of Surveying Engineering, 141 (4), 1–10. DOI: https://doi.org/10.1061/(ASCE)SU.1943-5428.0000144

Nowel, K., Kamiński, W. (2014). Robust estimation of deformation from observation differences for free control networks. Journal of Geodesy, 88 (8), 749–764. DOI: https://doi.org/10.1007/s00190-014-0719-7

Pelzer, H. (1971). Zur analyse geodätischer deformationsmessungen. Munich: Deutsche Geodätische Kommission.

Pelzer, H. (1974). Neuere ergebnisse bei der statistischen analyse von deformationsmessungen. In 14 FIG International Congress, Washington, DC.

Pennacchi, P. (2008). Robust estimate of excitations in mechanical systems using M-estimators–theoretical background and numerical applications. Journal of Sound and Vibration, 310 (4–5), 923–946. DOI: https://doi.org/10.1016/j.jsv.2007.08.007

Saidi, S., Houimli, H., Zid, J. (2017). Geodetic and GIS tools for dam safety: case of Sidi Salem dam (northern Tunisia). Arabian Journal of Geosciences, 10 (22), 505. DOI: https://doi.org/10.1007/s12517-017-3259-7

Savšek-Safić, S., Ambrožič, T., Stopar, B., Turk, G. (2006). Determination of point displacements in the geodetic network. Journal of Surveying Engineering, 132 (2), 58–63. DOI: https://doi.org/10.1061/(ASCE)0733-9453(2006)132:2(58)

Scaioni, M., Marsella, M., Crosetto, M., Tornatore, V., Wang, J. (2018). Geodetic and remote-sensing sensors for dam deformation monitoring. Sensors, 18 (11), 3682. DOI: https://doi.org/10.3390/s18113682

Setan, H., Som, Z. A. M., Idris, K. M. (2003). Deformation detection of lightweight concrete block using geodetic and non-geodetic methods. In 11th FIG Symposium on Deformation Measurements, May 25–28, 2003, Greece.

Setan, H., Singh, R. (2001). Deformation analysis of a geodetic monitoring network. Geomatica, 55 (3), 333–346. DOI: https://doi.org/10.5623/geomat-2001-0039

Taşçi, L. (2008). Dam deformation measurements with GPS. Geodesy and Cartography 34 (4), 116–121. DOI: https://doi.org/10.3846/1392-1541.2008.34.116-121

Taşçi, L. (2010). Analysis of dam deformation measurements with the robust and non-robust methods. Scientific Research and Essays, 5 (14), 1770–1779.

Wiśniewski, Z. (2009). Estimation of parameters in a split functional model of geodetic observations (M split estimation). Journal of Geodesy, 83 (2), 105–120. DOI: https://doi.org/10.1007/s00190-008-0241-x

Wiśniewski, Z. (2010). M split (q) estimation: estimation of parameters in a multi split functional model of geodetic observations. Journal of Geodesy, 84 (6), 355–372. DOI: https://doi.org/10.1007/s00190-010-0373-7

Xiao, R., Shi, H., He, X., Li, Z., Jia, D., Yang, Z. (2019). Deformation monitoring of reservoir dams using GNSS: an application to south-to-north water diversion project, China. IEEE Access, 7, 54981–54992. DOI: https://doi.org/10.1109/ACCESS.2019.2912143

Yavaşoğlu, H. H., Kalkan, Y., Tiryakioğlu, İ., Yigit, C. O., Özbey, V., Alkan, M. N., Bilgi, S., Alkan, R. M. (2018). Monitoring the deformation and strain analysis on the Ataturk Dam, Turkey. Geomatics Natural Hazards and Risk, 9 (1):94–107. DOI: https://doi.org/10.1080/19475705.2017.1411400

Yigit, C. O. (2016). Experimental assessment of post-processed kinematic precise point positioning method for structural health monitoring. Geomatics Natural Hazards and Risk, 7 (1), 360–383. DOI: https://doi.org/10.1080/19475705.2014.917724

Yigit, C. O., Alcay, S., Ceylan, A. (2016). Displacement response of a concrete arch dam to seasonal temperature fluctuations and reservoir level rise during the first filling period: evidence from geodetic data. Geomatics Natural Hazards and Risk, 7 (4), 1489–1505. DOI: https://doi.org/10.1080/19475705.2015.1047902

Konakoğlu B. (2020). Analysis of dam deformation with robust weight functions. Geodetski vestnik, 64 (2), 196-213. DOI: https://doi.org/10.15292/geodetski-vestnik.2020.02.196-213

Assist. prof. dr. Berkant Konakoglu
Amasya University, Technical Sciences Vocational School
TR-05100 Amasya, Turkey
e-mail: berkantkonakoglu@amasya.edu.tr